

Article

Design and Validation of a Low-Cost Structural Health Monitoring System for Dynamic Characterization of Structures

David Caballero-Russi ^{1,*} , Albert R. Ortiz ², Andrés Guzmán ³  and Carlos Canchila ⁴

¹ Department of Civil and Environmental Engineering, The Pennsylvania State University, University Park, PA 16802, USA

² School of Civil Engineering and Geomatics, Universidad del Valle, Cali 760032, Colombia; albert.ortiz@correounivalle.edu.co

³ Department of Civil and Environmental Engineering, Universidad del Norte, Puerto Colombia 081007, Colombia; faguzman@uninorte.edu.co

⁴ Department of Civil, Construction and Environmental Engineering, The University of Alabama, Tuscaloosa, AL 35487, USA; ccanchilamartinez@crimson.ua.edu

* Correspondence: dec5536@psu.edu; Tel.: +1-814-777-7598

Abstract: Structural Health Monitoring (SHM) is essential to identifying problems that may cause human and material losses produced by disastrous and unexpected structural failures. The dynamic characterization of civil structures adopting SHM systems provides, at a particular moment, accurate information about the current structural response. When considering a proper SHM strategy and affordable economic investment for the maintenance required by structures, it is possible to safeguard the original structural parameters and avoid potential failures. However, traditional SHM systems are not desirable due to the large economic investments involved and demand for exhausting fieldwork. This research presents the design, implementation, and validation of a low-cost SHM system composed of a Wireless Sensor Network (WSN) and a base station in order to identify dynamic properties from the measured structural response. A set of small- and full-scale experimental tests were conducted to validate the WSN system using a wired traditional SHM system. Vibration data recorded through the low-cost SHM system were processed and compared to determine the natural frequencies, mode shapes, and damping properties of different structures by computing modal identification techniques, frequency analysis, and logarithmic decrement. The obtained dynamic characterization results from small- and full-scale experimental testing conclude that the low-cost SHM system can reliably identify the dynamic properties of the tested structures. This proposal provides an inexpensive, functional, and innovative alternative for SHM regarding traditional monitoring systems.

Keywords: Structural Health Monitoring (SHM); dynamic characterization; structural response; low-cost SHM system; Wireless Sensor Network (WSN)



Citation: Caballero-Russi, D.; Ortiz, A.R.; Guzmán, A.; Canchila, C. Design and Validation of a Low-Cost Structural Health Monitoring System for Dynamic Characterization of Structures. *Appl. Sci.* **2022**, *12*, 2807. <https://doi.org/10.3390/app12062807>

Academic Editors: Mariusz Jaśniok, Maria Sozanska and Zbigniew Perkowski

Received: 1 December 2021

Accepted: 22 December 2021

Published: 9 March 2022

Publisher's Note: MDPI stays neutral with regard to jurisdictional claims in published maps and institutional affiliations.



Copyright: © 2022 by the authors. Licensee MDPI, Basel, Switzerland. This article is an open access article distributed under the terms and conditions of the Creative Commons Attribution (CC BY) license (<https://creativecommons.org/licenses/by/4.0/>).

1. Introduction

Structural Health Monitoring (SHM) aims to identify the response of a structural or mechanical system to detect and assess the severity of any damage caused by natural hazard events and ambient conditions in the short-term and long-term [1,2]. Since the physics and dynamic properties of civil structures are often unknown, their structural efficiency and usable lives may be compromised under different circumstances. Structural failures, material deterioration, and the influence of loading patterns such as winds, earthquakes, and hurricanes, are factors that undermine the structural health condition and increase uncertainties about the performance and safety of engineering infrastructure [3]. For these reasons, it is essential to grasp how civil structures respond over time in order to make preventive and appropriate decisions, preserving the welfare of these engineering projects.

It is beneficial to minimize the uncertainty of the behaviors of materials, loading conditions, and structural performance during the service lives of structures. Thus, evaluating

the construction process's quality and validating the computational structural designs is relevant to the initial conditions of an infrastructure project, which should then be subjected to strict procedures of inspection and SHM strategies [4].

Although non-destructive evaluation testing has been carried out on structures, a manageable and efficient evaluation approach, the deterioration of structures demands comprehensive assessments of the prevailing condition of such structures, employing effective monitoring and maintenance strategies [5]. Since the first SHM implementations in previous decades, the traditional SHM system was used and conceived principally as a base station and a sturdy wired-sensors network. In addition to the high purchase and maintenance costs, these characteristics involve particular difficulties in relocating and installing the monitoring system components [6].

As civil structures age, they progressively deteriorate and may suddenly collapse; these conditions are often assumed improperly by people in charge of the operation and maintenance of civil structures. Owners neglect to implement an adequate SHM system because the economic implications are considerably expensive and "inconvenient". The expensive components of wired traditional monitoring systems consist of data acquisition and transmission systems, wired devices, sensor classes, and fieldwork costs. Furthermore, the setting times of these monitoring systems can be hours or even days, depending on the structural geometry and spatial location of the SHM plan [7]. If SHM systems were to be considered for existing infrastructure and design standards of new civil structures, detecting the decaying infrastructure and regulating a formal methodology needed to identify structural damage in future scenarios would be possible [8].

The simplified installation and reduction in economic investments provided by WSN monitoring systems with innovative features have made them attractive, efficient alternative strategies for SHM. The development of technical characteristics such as advanced sensor technology, large-range wireless communication protocols, robust computational capacity, and low-power consumption have allowed taking SHM from small-scale experimental testing to the structural monitoring of massive infrastructure projects, including historic buildings and industries, footbridges, and highways [9].

This paper proposes the design, implementation, and validation of a low-cost SHM system capable of measuring the structural responses and identifying the dynamic properties of different structural systems using inexpensive technological devices and standard dynamical identification techniques. Thus, the extraction of the modal parameters found by this system provides accurate information for, subsequently, assessing the health condition of a civil structure and detecting damage scenarios. The present study provides an attractive cost-benefit alternative and effortless methodology for SHM regardless of the complexity of civil infrastructure. The development of the low-cost SHM system represents a relevant contribution to interdisciplinary research between SHM and electronic communications.

2. Background

2.1. Structural Health Monitoring

The report LA-13975-MS published by Los Alamos National Laboratory suggests three prime guidelines to describe a methodology for SHM: structural condition examination, experimental setup and SHM system characteristics, and feature extraction [10]. The structural condition examination is necessary to identify the causes of the structural monitoring inquiry. Then, it is possible to determine the relevant structural parameters for testing and the ambient and operational surroundings of the civil structure. The experimental setup and SHM system characteristics include the measurements provided; testing methods; and sensor quantity, arrangement, and features. Moreover, data acquisition, storage, and transmission systems are essential components selected according to sampling frequency, data size, and environmental conditions. Finally, the feature extraction is carried out through the information already recorded in order to perform data processing, and consequently, compute system identification and damage detection algorithms regarding the structural parameters at issue.

Vibration-based SHM comprehends system identification as one of the most relevant approaches for smart infrastructure. In order to perform a system identification approach, digital signal processing techniques play an essential part in information from sensors. Thus, the more accurate and efficient the signal processing techniques in the system identification process, the more reliable the structural health condition assessment of the civil structure. The success of vibration-based SHM strategies relies on embracing digital signal processing and structural health condition assessments to preserve civil engineering structures from natural and man-made hazards and improve community resilience [11,12].

Historically, aerospace, civil, and mechanical engineering have been considered the most progressive work fields regarding SHM [1]. SHM strategies require a critical component to reach highly-accurate outcomes: technological devices with specific hardware and software characteristics for studying the response of the structure and its operational ambience. The SHM framework enables thorough tracking of the response of a structure over its lifetime, recording permanently or periodically information about structural properties from monitoring systems [3]. In this regard, SHM systems comprise assemblies of particular elements; each SHM system component includes specific features and accomplishes particular tasks. However, there is a group of conventional but significant characteristics required for every monitoring system: power consumption, programming assignments, signal acquisition and conditioning capabilities, data storage and processing capabilities, a communication protocol, and numerical computing techniques, among others.

The deterioration detection of civil structures by SHM strategies empowers the decision-making of further structural interventions on time. Regarding traditional SHM implementations, the Bill Emerson Memorial Bridge, located in Missouri, United States, is a 1210-m cable-stayed structure and carries a wired SHM monitoring system (placed in 2005) made up of 84 seismic accelerometers for evaluating the performance and checking design parameters, and additionally, providing information for future design evaluation [13]. In addition, the Tsing Ma Bridge is a 2132-m suspension bridge located in Hong Kong, China, holding an SHM system (installed in 1997) accompanied by a high-density arrangement of 110 dynamic strain wired gauges for the evaluation of internal forces at bridge cross-sections and bearings [14].

Seeking to reshape SHM strategies in a more attractive, affordable, and efficient way, WSNs have been used for SHM development due to their minor costs, rapid experimental setups, and more accurate computational techniques. As one of the most representative low-cost SHM implementations, the Jindo Bridge is a 484-m cable-stayed structure located in Jindo, South Korea, monitored by a smart WSN since 2009. This monitoring system consists of two base stations and 70 measuring nodes; every measuring node has a high-efficiency computational device, Imote2 (Imote2 IBB2400AC. Moog Inc., New York, NY, USA); multi-scale sensor boards; and a battery pack (7.5 V supply voltage). The multi-scale sensor boards include analog accelerometers with a measurement range of ± 2.0 g, a 16-bit analog-to-digital converter (ADC) signal digitizer, 3-D ultra-sonic anemometers, and sensors of temperature, humidity, and light [15]. The Torre Aquila tower is a 31-m tall medieval structure settled in Trento, Italy, where a WSN was installed for health monitoring in 2008. The configuration of the WSN involves a base station and 16 measuring nodes, each of which comprises a 12-bit ADC processor module 3MATE! (3MATE!. TRETEC S.R.L., Trento, Italy), a portal battery (6.0 V supply voltage), and a sensor categorized by type of analysis: an ambient conditions sensor (temperature, relative moisture, and luminosity), a micro-electromechanical systems (MEMS) accelerometer with a measurement range of ± 1.5 g, or a strain gauge [16]. Likewise, the Golden Gate Bridge is a suspension structure of a 1280-m main span located in San Francisco Bay, United States, examined by an SHM WSN since 2007. This wireless monitoring system is composed of a single base station and 64 nodes arranged throughout the main span and tower of the bridge. Every deployed node, powered by 8.0 V supply voltage, includes a MICAz Mote (MICAz Mote. Moog Inc., New York, NY, USA) along with a sensor board: two MEMS accelerometers with a 16-bit antialiasing filter and a measurement range of ± 2.0 g, and a thermometer [17].

The primary motivation for implementing WSNs is their extraordinary cost-effectiveness. Table 1 presents the economic investments required for some relevant infrastructure projects adopting both types of SHM systems.

Table 1. Comparison of costs for SHM systems.

Monitored Structure (Year)	Type of SHM System	Estimated Cost of SHM System (USD)	Estimated Cost per Node (USD)
Tsing Ma Bridge (1997)	Traditional	\$8,000,000	\$26,667
Bill Emerson Memorial Bridge (2005)	Traditional	\$1,500,000	\$17,857
Golden Gate Bridge (2006)	Wireless network	\$38,400	\$600
Aquila Tower (2008)	Wireless network	\$1429	\$89
Jindo Bridge (2009)	Wireless v	\$35,000	\$500

2.2. Dynamic Characterization and Processing Techniques

The classic dynamic response is defined by a physic model considering the mass, stiffness, and damping properties of a linear time-invariant structural system to an external force. The following second-order differential Equation (1) represents the harmonic vibration response of viscous damping multi-degree-of-freedom structural systems [18]:

$$[M]\{\ddot{x}\} + [C]\{\dot{x}\} + [K]\{x\} = \begin{cases} p(t) = 0 \\ p(t) = p_0 \sin(\omega t) \end{cases} \quad (1)$$

where M is the mass matrix, C is the damping matrix, K is the stiffness matrix, x is the vector of displacement of the system, $p(t)$ is known as the external dynamic force, p_0 is the force amplitude, ω is the exciting frequency, and t is the time instant.

For the estimation of the damping properties, the free-vibration response of the system only considers the response thereof to initial conditions of displacement and velocity as the external dynamic force disappears ($p(t)$ is 0 at Equation (1)). Thus, the damping ratio ζ takes a relevant role in the decaying phenomena of the motion. As outlined in [18], the relation between acceleration \ddot{x} , at t time, is independent of time history, so this definition enables the damping ratio ζ calculation through logarithmic decrement as:

$$\delta = Ln \left(\frac{\ddot{x}_1}{\ddot{x}_{j+1}} \right) = \frac{2\pi j \zeta}{\sqrt{1 - \zeta^2}} \quad (2)$$

where j is the number of vibration periods proceeded.

The modal analysis consists of a methodology for determining the dynamic characteristics of a system in terms of natural frequencies, mode shapes, and damping ratios in order to formulate a mathematical model that estimates the dynamic response of a structure. Concerning this subject, the modal analysis framework considered in this paper involves operational modal analysis (OMA), adopting the frequency domain decomposition (FDD) technique and performing the vibration mode correlation by modal assurance criterion (MAC). Furthermore, the time–frequency analysis was conducted to study the dynamic performance of the system across time.

FDD technique relies on the singular value decomposition (SVD) of the power spectral density matrix G_{yy} . The power spectral density matrix G_{yy} is decomposed into auto-power spectral density functions corresponding to a single-degree-of-freedom system [19]. Then, it is possible to estimate natural frequencies and modes shapes of vibration modes as [20]:

$$G_{yy}(w_i) = U_i S_i U_i^H \quad (3)$$

where, for every frequency line w_i , U_i is the matrix of the m singular vectors u_{il} , S_i is the diagonal matrix of the m singular values s_{il} considering l from 1 to m , and H denotes the transpose conjugate complex. This approach is accurate when the input excitation is white noise, the structure has light damping properties, and mode shapes from close vibration modes are well separated [21]. To compare the identified mode shapes, MAC is performed

between test and analytical modal vectors to ascertain the degree of consistency among mode shapes, as described in Equation (4) [22]:

$$\text{MAC}(r, q) = \frac{|\{\varphi_A\}_r^T \{\varphi_X\}_q|^2}{(\{\varphi_A\}_r^T \{\varphi_A\}_r)(\{\varphi_X\}_q^T \{\varphi_X\}_q)} \quad (4)$$

where $\{\varphi_A\}_r$ is the analytical modal vector corresponding to mode r , $\{\varphi_X\}_q$ denotes the test modal vector corresponding to mode q , and T represents the transpose matrix. For the outreach of this paper, the considered MAC acceptance level was 0.80 as a typical value suggested in [23]. Larger values than 0.80 mean high significance consistency, whereas small values represent a poor correlation between mode shape vectors.

Time–frequency analysis was employed to identify and assess the natural frequencies of the tested structures throughout time. This technique enables tracking the frequency content of civil structures over time windows to retrieve the external frequencies (as operational, ambient, and noisy frequencies) from the original dynamic system response. Spectrogram methods commonly are based on discrete Fourier transform (DFT), computed through [24]:

$$x(n) = \sum_{k=0}^{N-1} c_k e^{\frac{J2\pi kn}{N}} \quad (5)$$

where $x(n)$ is the discrete periodic signal in time n , N is the signal period, J is the complex number, and c_k are the Fourier series coefficients.

3. Methodology

The validation of the low-cost SHM system was conducted by comparing and evaluating a set of small- and full-scale experimental tests using a reference SHM system. The experimental tests aimed to estimate the outreach, ascertain the performance, and identify the weaknesses of the low-cost monitoring system according to different ambient conditions. The analysis and the characterization of the dynamic properties of the structures were carried out considering a deterministic approach and white noise input excitation to ambient vibrations.

Our methodology addressed data gathering, preprocessing, and processing and evaluation for every experimental testing case. The flowchart of this framework is shown in Figure 1.

3.1. Structural Health Monitoring Systems

3.1.1. Low-Cost Structural Health Monitoring System

The vibration-based SHM system is composed of a WSN, made up of independent measuring nodes, and a base station. This wireless monitoring system records the response of the structure in terms of linear accelerations. When the information is collected, the vibration data are communicated towards the base station to analyze and characterize the dynamic properties of the structure. The low-cost SHM system runs short-term SHM testing, and its radiofrequency technology enables data communication.

The low-cost SHM system consists of three main elements: the measuring node, the WSN, and the base station.

The heart of the low-cost SHM system is the measuring node. It comprises a microprocessor platform, Raspberry Pi 3B+, and a MEMS accelerometer, ADXL355. Raspberry Pi 3B+ is a system on chip (SoC) electronic device that carries a Broadcom BCM2837B0 Cortex-A53 processor (64-bit) and 1 GB LPDDR2 RAM. The microprocessor platform holds versatile, reliable, low-power, and low-cost hardware. This computational device requires a 5.0 V input power and costs about USD 38.5 [25,26]. The microprocessor platform Raspberry Pi 3B+ performs three primary functions: supplying power to the measuring nodes, responding to data acquisition requests, and data storage and communication. The computer module

is a Linux Ubuntu MATE 18.04 LTS operating system, and it has a 16 GB SD card. The ADXL355 MEMS accelerometer is a triaxial digital device that includes a 20-bit ADC, has a $3.9 \mu\text{g}/\text{LSB}$ sensibility, and employs a $\pm 2.048 \text{ g}$ full-scale range. Furthermore, the ADXL355 MEMS sensor is a low noise density, low-power, and low-cost sensor device. This digital device features a 3.3 V input power and costs about USD 35.0 [27,28]. The triaxial sensor was used to acquire signals at 250 Hz. Figure 2 shows the composition of the proposed measuring node.

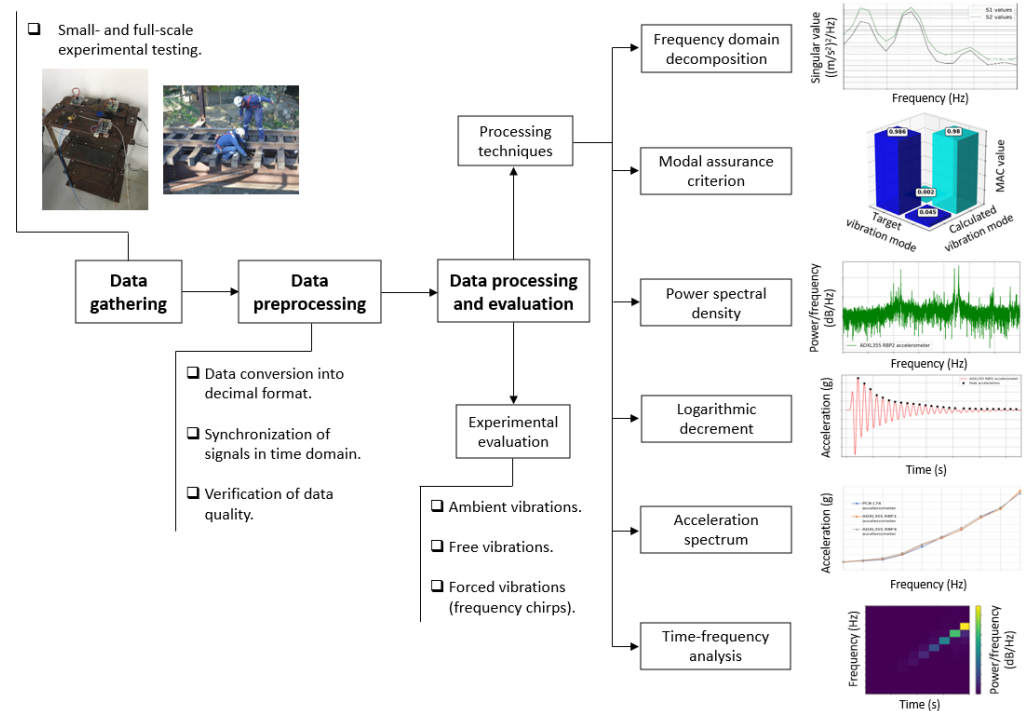


Figure 1. Descriptive diagram of the methodology framework.

The proposed WSN topology was considered to have star architecture. The star network topology has a logic map exclusively communicate information between the base station and every measuring node. Concerning this network topology, the scalability of the low-cost SHM system allows adding measuring nodes easily [9]. The local communication between the microprocessor platform and accelerometer implements an I2C communication protocol, consisting of a synchronous serial interface bus that directly connects these electronic devices [29]. For this purpose, jumpers attached to the microprocessor platform and accelerometer GPIO pin headers were needed [28].

Regarding the time synchronization of the WSN, Network Time Protocol (NTP) is employed to sync the clock of the Raspberry Pi 3B+ via the Internet with servers distributed worldwide [30]. As soon as the Raspberry Pi 3B+ gets an Internet connection, the time information request is sent to the server for clock synchronization.

The functioning of the low-cost SHM system comprises two stages: data acquisition and communication, and dynamic characterization. These functioning stages occur consecutively. The Raspberry Pi 3B+ triggers the ADXL355 accelerometer through an automated request programmed in the startup file. Once the accelerometer acquires the vibration data, the Raspberry Pi 3B+ of the measuring node carries out the storage and communication processes. Afterwards, from the base station computer, it is possible to handle the signal processing and the dynamical system characterization in a pseudo-real time step. Figure 3 shows the function block diagram of the low-cost SHM system.

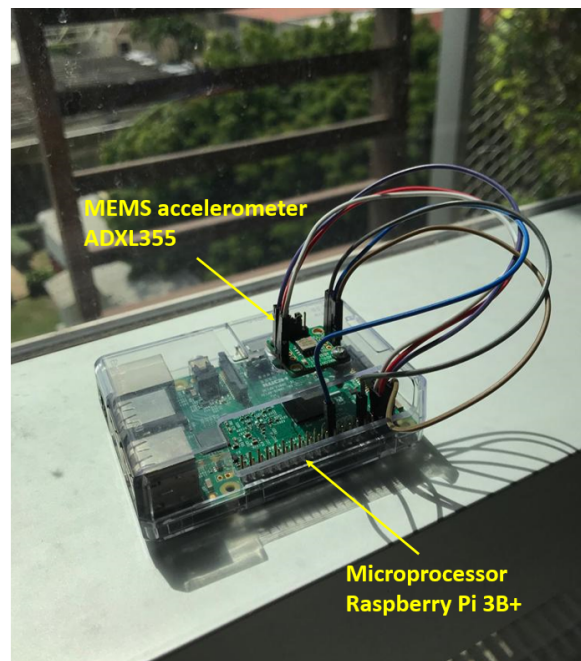


Figure 2. Measuring node of the low-cost SHM system.

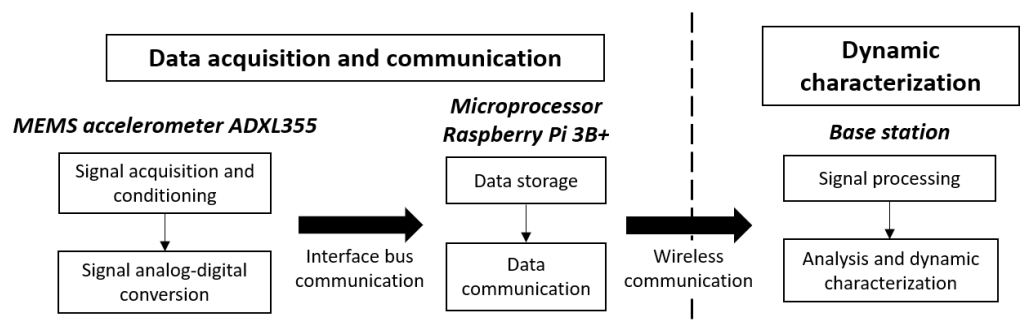


Figure 3. Function block diagram of the low-cost WSN monitoring system.

For the data acquisition and communication stage, the input parameters of the measurement (such as record time, sampling frequency, and data storage) are set manually by remote connection from the base station. The wireless communication technology related to the monitoring system held to the IEEE 802.11 standard protocol on the 2.4 GHz frequency band [25]. According to the function scheme, the Raspberry microprocessor Pi 3B+ sends the data acquisition request to the ADXL355 accelerometer for the analog signal acquisition. Then, the signal conditioning adapts and addresses the analog signal through the ADC converter. In this regard, the accelerometer FIFO buffer arranges and saves the digital signal in a 20-bit integer format. Simultaneously, the Raspberry Pi 3B+ solicits the data acquired through the interface bus communication and saves the information temporarily. Once the testing finishes, the stored data are communicated remotely from the base station via VNC Connect. The user at the base station adequately addresses this data transmission inquiry. After the base station receives the information from all measuring nodes of the WSN, it is possible to process and analyze the dataset in order to characterize the dynamic properties of the structure monitored.

3.1.2. Reference Structural Health Monitoring System

The reference SHM system is a wired traditional monitoring system. This reference monitoring system monitors the structural response in terms of linear accelerations by employing wired accelerometers, a data acquisition system, and a computer. The CompactDAQ data acquisition system platform of National Instruments (NI) includes two

NI 9234 signal acquisition modules, an energy cable, and a USB carrier. This whole data acquisition system platform costs about USD 4625. The signal acquisition module is a four-channel dynamic signal device holding a 24-bit ADC and acquires data at a sample rate of 1500 Hz [31]. Furthermore, the wired accelerometers are PCB Piezotronics piezoelectric sensors, and their features are presented in Table 2.

Table 2. Technique features of the PCB Piezotronics accelerometers.

Feature	Accelerometers		
Model	356B18	356B18	333B50
Measurement axes	Triaxial	Triaxial	Uniaxial
Reference name	PCB L94	PCB L74	PCB L12
Sensitivity (mV/g)	1000	1000	1000
Measurement range (V)	±5.0	±5.0	±5.0
Frequency range ±5.0% (Hz)	0.5–3000	0.5–3000	0.5–3000
Cost (USD)	\$1764	\$1764	\$598.5

3.2. Descriptions of the Tests

In order to assess the performance of the low-cost SHM system, we performed tests categorized into: small- and full-scale testing. The experimental setup, data processing techniques, and engineering parameters are defined for every testing case.

3.2.1. Small-Scale Testing

Two experiments were conducted in the structural laboratory at Universidad del Norte: The first experiment resulted in the analysis of vibration data recorded from a set of frequency chirps by a shaking table, whereas the second experiment considered the dynamic characterization of a flexible structure.

- *Shaking Table Tests:* The Quanser Shake Table II is a single-axis motion simulator operated with open architecture software. The shaking table can reproduce sinusoidal and frequency chirp motions and pre-loaded accelerograms of real earthquakes employing a plan dimension platform of 61×46 cm with a total height of 13 cm. The simulator allows an operational weight of 7.5 kg for an acceleration of 2.5 g [32]. This test ensued in the analysis of data vibrations recorded from frequency chirps performed by the shaking table with different displacements according to distinct frequencies from 0.5 to 5.0 Hz, 0.5 Hz increments, using a sinusoidal excitation. For the frequency chirps, 0.10 cm, 0.25 cm, 0.50 cm, and 0.75 cm displacements were considered. Two wireless measuring nodes and one piezoelectric accelerometer were used to deploy the low-cost and reference SHM systems during testing. The accelerometer arrangement over the Shake Table II platform is presented in Figure 4.

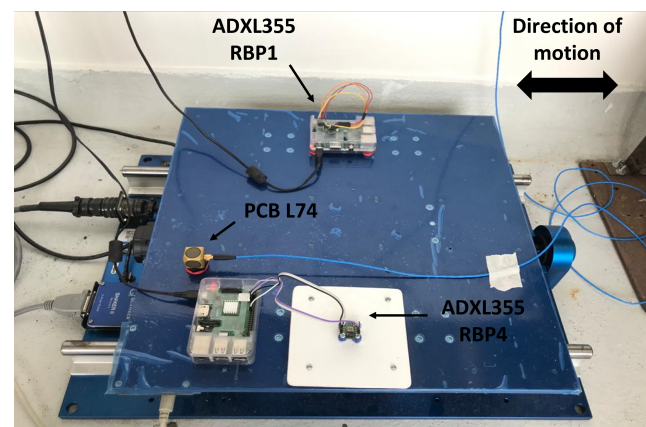


Figure 4. Experimental setup of the frequency chirps on Quanser Shake Table II.

The comparison of the acceleration time series between the PCB L74 accelerometer and the ADXL355 RBP1 and ADXL355 RBP4 accelerometers was conducted through three types of acceleration spectrum in the direction of motion: from the original sampling frequency, from 100 Hz resampling frequency, and from the mean of the highest 100 acceleration peaks from 100 Hz resampling frequency. Then, the RMS error of vibration data was calculated from wireless measuring nodes accelerometers regarding the piezoelectric accelerometer. Finally, spectrograms were computed for time–frequency distribution analysis.

- *Flexible Structure Monitoring*: The tested two-story structure consists of 15×10 cm acrylic plates as floor systems and 80-cm aluminum leaves as lateral support elements. The story height is 40 cm, and the structure was constrained at the bottom above a stiff desk by clamps. The flexible structure was represented as a two-degree-of-freedom (2-DOF) shear frame for the testing. The dynamic characterization of the structure was carried out through ambient and free-vibration records from the structural response, excited by random displacements on the highest DOF. The experimental setup involved a measurement channel on every DOF, and every measurement channel had a measuring unit for each SHM system. Figure 5 shows the aluminum structure, the experimental scheme of the testing, and the sensor array on DOF 2 of the flexible structure.

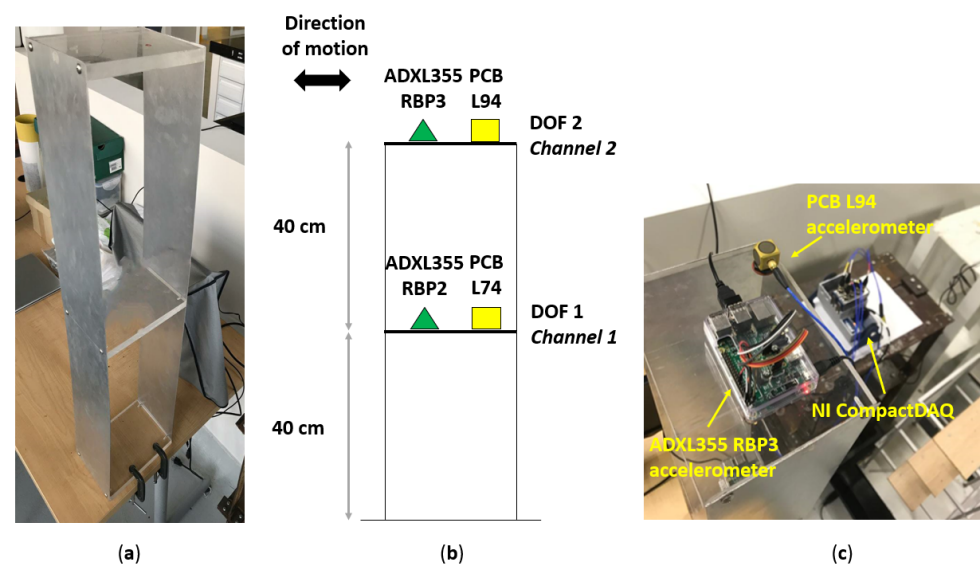


Figure 5. Flexible structure monitoring: (a) Two-story flexible structure. (b) Experimental setup. (c) Location of measurement channel 2.

The vibration data of the reference SHM system were resampled at a 250 Hz sampling rate to perform the dynamic characterization of signals of frequency content without bias. As a 2-DOF dynamical system response was measured, it was possible to identify dominant vibration modes corresponding to the directions of motion. Ambient vibration data were processed using the FDD technique to estimate natural frequencies and mode shapes. Likewise, free-vibration data were processed by the logarithmic decrement method to calculate modal damping ratios.

3.2.2. Full-Scale Testing

Two experiments were carried out on different large civil structures: The first experiment consisted of monitoring natural frequencies on a structural slab during demolition work, whereas the second experiment consisted of the dynamic characterization of a railway bridge during its operation.

- *Beam Demolition Monitoring*: The reinforced concrete (RC) beam (later demolished), or so-called check-in beam, was a lateral support element of a lightweight RC slab. The

prestressed concrete slab has five primary spans of 24-m joists placed in the lightweight RC slab transverse direction. The 49-m check-in beam supported 30 prestressed concrete joists. Prior to the demolition work, an RC girder was constructed to resist the lightweight RC slab laterally and replace the check-in beam. The prestressed concrete slab was monitored to evaluate whether the vibrations of the demolition would produce significant disturbances to the current service zone of the airport, and thus identify the stiffness changes that may compromise the stability of the structure. The SHM strategy was carried out on the central joist, for each span, through ambient and forced vibration records during the TE 1500-AVR Hilti demolition hammer operation, whose impact frequency was 1620 impacts/minute (27.0 Hz) [33]. A measuring node was installed at the base of the central joist mid-length to every span (Figure 6). The demolition work and structural monitoring were completed at once, span by span, as pointed in Figure 7. Thus, the base station moved continuously throughout the check-in beam demolition.

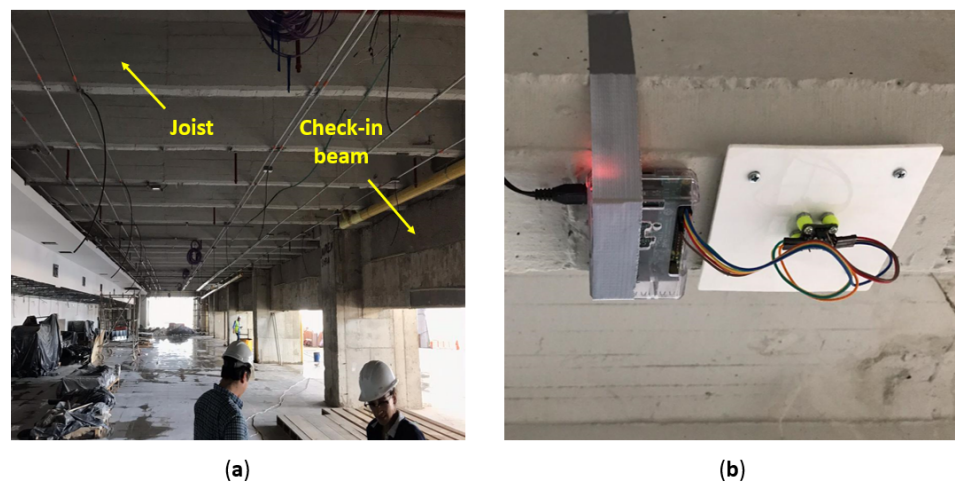


Figure 6. Beam demolition monitoring: (a) Joists of the slab and check-in beam. (b) Measuring node.

The vibration data were resampled at 70 Hz, a frequency that includes the dominant vibration modes. From the lightweight RC slab response measured, natural frequencies were identified and monitored by power spectral densities and spectrograms before and during the demolition work. The frequency analysis implemented for the prestressed concrete slab considered just the vertical transverse direction of the joists from the slab using the low-cost SHM system.

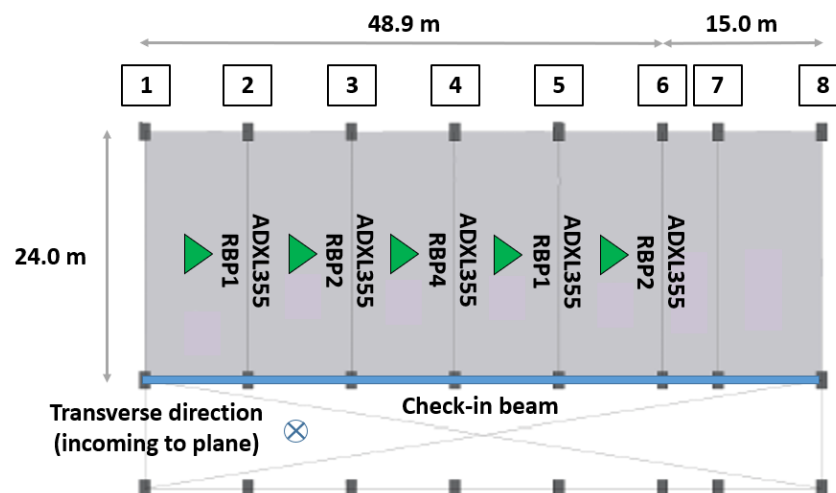


Figure 7. Experimental setup of the beam demolition monitoring.

- *Railway Bridge Monitoring*: The test bridge is a single-span steel structure composed of a tridimensional truss, connected along the top seam by a latticework and along the bottom seam by structural steel members. The steel structure has one 44.0-m span in the longitudinal direction, a deck width of 5.3 m, and a height of 9.0 m. Figure 8 presents a perspective image of the steel structure.



Figure 8. Steel structure of the railway bridge.

The railway bridge was defined as a 6-DOF dynamic system for testing: 3 vertical and transverse DOF. The dynamic characterization of the structure was conducted for both vertical and transverse directions individually through ambient, forced, and free-vibration records from the structural responses elicited by diverse train traffic (classified by velocity, loading capacity, and type of train) on the steel bridge. The experimental setup consisted of three measurement channels composed of a vertical and transverse DOF. On this subject, the measurement channels were set to L/4, L/2, and 3/4L of the bridge length from the base station placement, positioning the measuring nodes between the railway sleepers and above the top flange of the bottom structural steel members as shown in Figure 9. The locations of the measuring nodes for channel 1 and the base station (located at the south side of the structure) are pointed to in Figure 10.

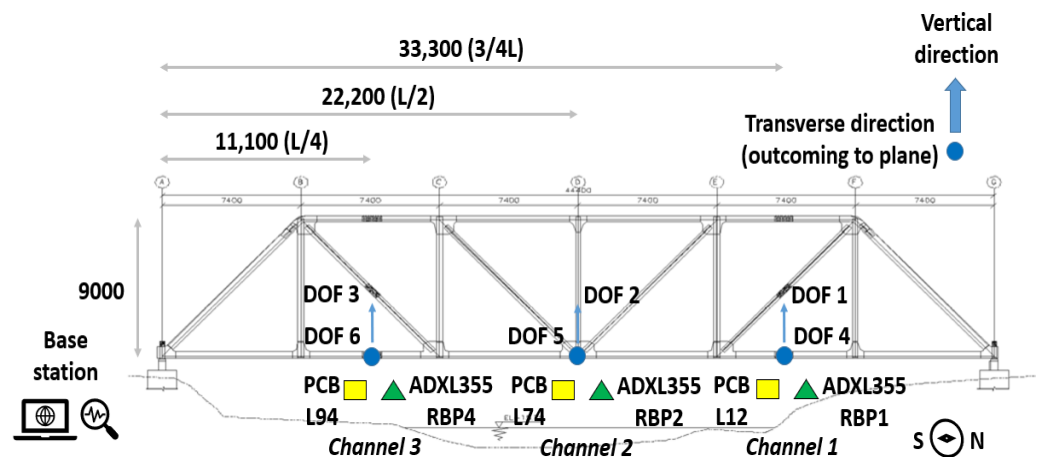


Figure 9. Experimental setup of the testing conducted on a steel structure (lateral view). Dimensions in mm.

The vibration data of the reference SHM system were resampled at 250 Hz to, as described above, process and compare digital signals from unbiased frequency ranges. As the 6-DOF dynamical system response was measured, it was possible to identify vertical and transverse dominant vibration modes of the railway bridge. Ambient vibration data were processed using the FDD decomposition technique to determine natural frequencies and

mode shapes. Likewise, free-vibration data were processed by the logarithmic decrement method to estimate modal damping ratios.



Figure 10. Railway bridge monitoring: (a) Location of measurement channel 1. (b) Base station of testing.

The DOF 4, toward the plane and located in the measurement channel 1, was just measured by the ADXL355 RBP1 accelerometer, since the uniaxial PCB L12 accelerometer, located in the same place, was deployed for the DOF 1 (vertically).

4. Results and Validation

According to the tests described in the previous section, the results obtained are presented in this section.

4.1. Small-Scale Testing

The results reached from shaking table tests and flexible structure monitoring are introduced below to evaluate the performance of the low-cost SHM system for small-scale experimentation.

4.1.1. Shaking Table Tests

The acceleration spectra and fitting equations for the vibration dataset recorded from the 0.10 cm displacement frequency chirp by every accelerometer are presented in Figure 11. The first frequency of excitation (0.5 Hz) caused acceleration values higher than the acceleration amplitudes detected for the next three excitation frequencies (1.0, 1.5, and 2.0 Hz) in all accelerometers. This particular trend may be associated with an electric or mechanical issue on the shaking table that reproduces sinusoidal motions with low amplitude concerning these specific frequency levels. Despite the outlier accelerations registered for low excitation frequencies, the tendency of vibration data for every type of acceleration spectrum fit a linear pattern. The acceleration ranges, coefficients of determination R^2 of fitting equations, and RMS error for the set of 0.10 cm displacement acceleration spectra are shown in Table 3.

For the 0.25 cm displacement frequency chirp, the acceleration spectra and fitting equations for the vibration dataset according to every accelerometer are presented in Figure 12. The sinusoidal motion provided a more consistent acceleration value at 0.5 Hz of excitation, regarding the three excitation frequencies mentioned before, to all accelerometers. Unlike the linear trend fitted for the previous frequency chirp analysis, the acceleration spectra of each accelerometer showed amplitude increments following an exponential pattern. Table 4 summarizes the acceleration ranges, coefficients of determination R^2 of fitting equations, and RMS error for the set of 0.25 cm displacement acceleration spectra.

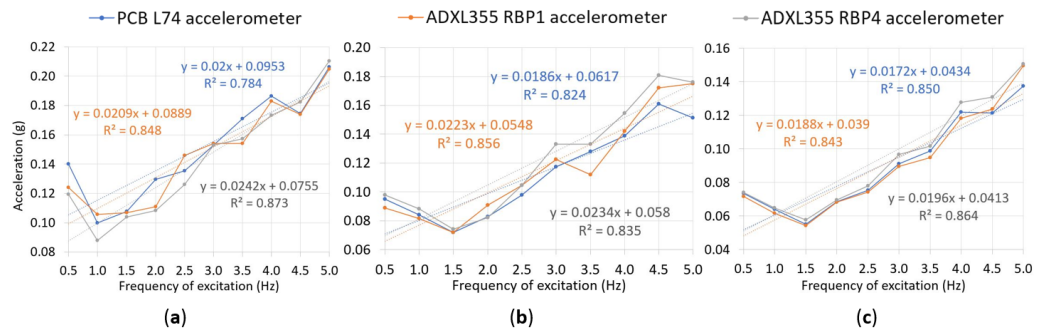


Figure 11. Acceleration spectra for the 0.10 cm displacement frequency chirp: (a) Maximum acceleration spectrum from original sampling frequency. (b) Maximum acceleration spectrum from 100 Hz resampling frequency. (c) Acceleration spectrum for the mean of the highest 100 acceleration peaks from 100 Hz resampling frequency.

Table 3. Summary of the results obtained from the 0.10 cm displacement frequency chirp.

Acceleration Spectrum	Accelerometer	Accelerations Range (g)	R ²	RMS Error (g)
Original sampling frequency	PCB L74	0.10–0.21	0.784	-
	ADXL355 RBP1	0.11–0.20	0.848	0.010
	ADXL355 RBP4	0.088–0.21	0.873	0.012
100 Hz resampling frequency	PCB L74	0.072–0.16	0.824	-
	ADXL355 RBP1	0.072–0.18	0.856	0.011
	ADXL355 RBP4	0.074–0.18	0.835	0.013
Highest 100 acceleration peaks mean	PCB L74	0.055–0.14	0.850	-
	ADXL355 RBP1	0.054–0.15	0.843	0.0043
	ADXL355 RBP4	0.058–0.15	0.835	0.0059

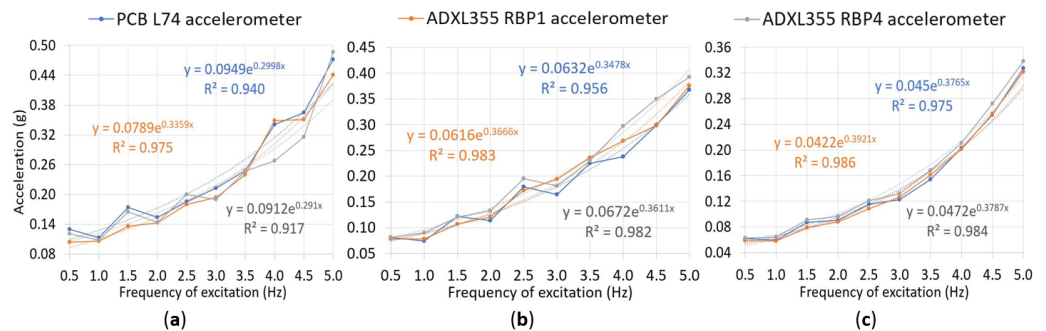


Figure 12. Acceleration spectra for the 0.25 cm displacement frequency chirp: (a) Maximum acceleration spectrum from original sampling frequency. (b) Maximum acceleration spectrum from 100 Hz resampling frequency. (c) Acceleration spectrum from the mean of the highest 100 acceleration peaks from 100 Hz resampling frequency.

For the 0.50 cm displacement frequency chirp, the acceleration spectra and fitting equations for the vibration dataset recorded by every accelerometer are presented in Figure 13. As occurred in the 0.25 cm displacement frequency chirp, the tendency of vibration data depicted for each type of acceleration spectrum fit an exponential pattern. The acceleration ranges, coefficients of determination R² of fitting equations, and RMS error for the set of 0.50 cm displacement acceleration spectra are shown in Table 5.

Table 4. Summary of the results obtained from the 0.25 cm displacement frequency chirp.

Acceleration Spectrum	Accelerometer	Accelerations Range (g)	R ²	RMS Error (g)
Original sampling frequency	PCB L74	0.11–0.47	0.940	-
	ADXL355 RBP1	0.10–0.44	0.975	0.020
	ADXL355 RBP4	0.11–0.49	0.917	0.030
100 Hz resampling frequency	PCB L74	0.074–0.37	0.956	-
	ADXL355 RBP1	0.078–0.38	0.983	0.015
	ADXL355 RBP4	0.081–0.39	0.982	0.028
Highest 100 acceleration peaks mean	PCB L74	0.059–0.33	0.975	-
	ADXL355 RBP1	0.058–0.32	0.986	0.0049
	ADXL355 RBP4	0.063–0.34	0.984	0.0093

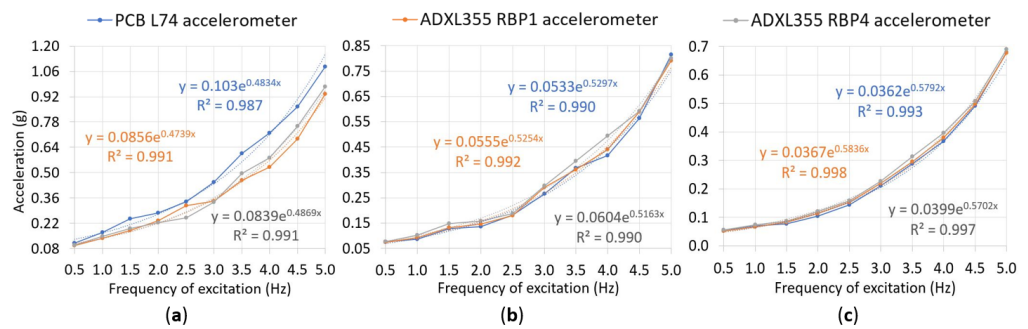


Figure 13. Acceleration spectra for the 0.50 cm displacement frequency chirp: (a) Maximum acceleration spectrum from original sampling frequency. (b) Maximum acceleration spectrum from 100 Hz resampling frequency. (c) Acceleration spectrum from the mean of the highest 100 acceleration peaks from 100 Hz resampling frequency.

Table 5. Summary of the results obtained from the 0.50 cm displacement frequency chirp.

Acceleration Spectrum	Accelerometer	Accelerations Range (g)	R ²	RMS Error (g)
Original sampling frequency	PCB L74	0.11–1.08	0.987	-
	ADXL355 RBP1	0.098–0.93	0.991	0.11
	ADXL355 RBP4	0.10–0.98	0.991	0.090
100 Hz resampling frequency	PCB L74	0.076–0.81	0.990	-
	ADXL355 RBP1	0.075–0.79	0.992	0.016
	ADXL355 RBP4	0.077–0.80	0.990	0.032
Highest 100 acceleration peaks mean	PCB L74	0.054–0.68	0.993	-
	ADXL355 RBP1	0.052–0.68	0.998	0.0077
	ADXL355 RBP4	0.056–0.69	0.997	0.017

The acceleration spectra and fitting equations for the vibration dataset from the 0.75 cm displacement frequency chirp according to every accelerometer are presented in Figure 14. The acceleration spectra for every accelerometer suggested amplitude increments following an exponential pattern. Table 6 summarizes the acceleration ranges, coefficients of determination R² of fitting equations, and RMS error for the set of 0.75 cm displacement acceleration spectra.

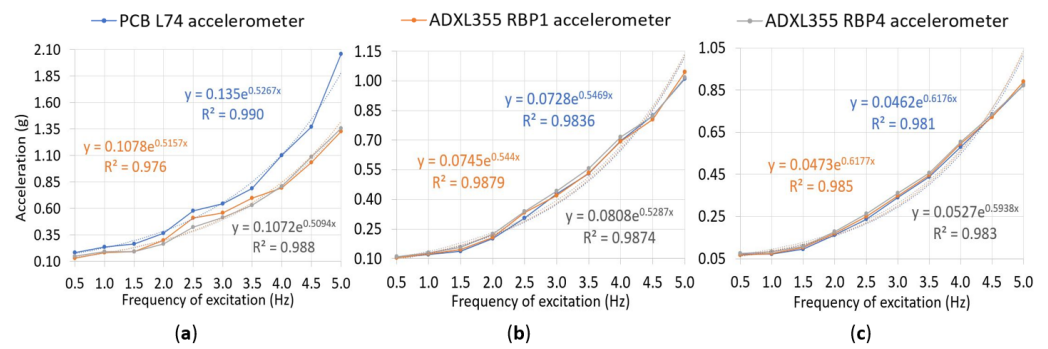


Figure 14. Acceleration spectra for the 0.75 cm displacement frequency chirp: (a) Maximum acceleration spectrum from original sampling frequency. (b) Maximum acceleration spectrum from 100 Hz resampling frequency. (c) Acceleration spectrum from the mean of the highest 100 acceleration peaks from 100 Hz resampling frequency.

Table 6. Summary of the results obtained from the 0.75 cm displacement frequency chirp.

Acceleration Spectrum	Accelerometer	Accelerations Range (g)	R ²	RMS Error (g)
Original sampling frequency	PCB L74	0.19–2.1	0.990	-
	ADXL355 RBP1	0.13–1.33	0.976	0.28
	ADXL355 RBP4	0.15–1.36	0.988	0.27
100 Hz resampling frequency	PCB L74	0.11–1.01	0.984	-
	ADXL355 RBP1	0.10–1.04	0.988	0.015
	ADXL355 RBP4	0.11–1.02	0.987	0.019
Highest 100 acceleration peaks mean	PCB L74	0.071–0.87	0.981	-
	ADXL355 RBP1	0.068–0.89	0.985	0.0091
	ADXL355 RBP4	0.076–0.87	0.983	0.016

Figures 15–18 reveal the frequency and energy content throughout the test in spectrograms for the frequency chirps. The energy released by these four frequency chirps increased as the displacement of the sinusoidal excitation incremented, following a staggered time–frequency distribution for all frequency chirps performed. The similarity of energy levels detected among the accelerometers is relevant evidence of the satisfactory performance from the low-cost SHM system regarding the traditional SHM system.

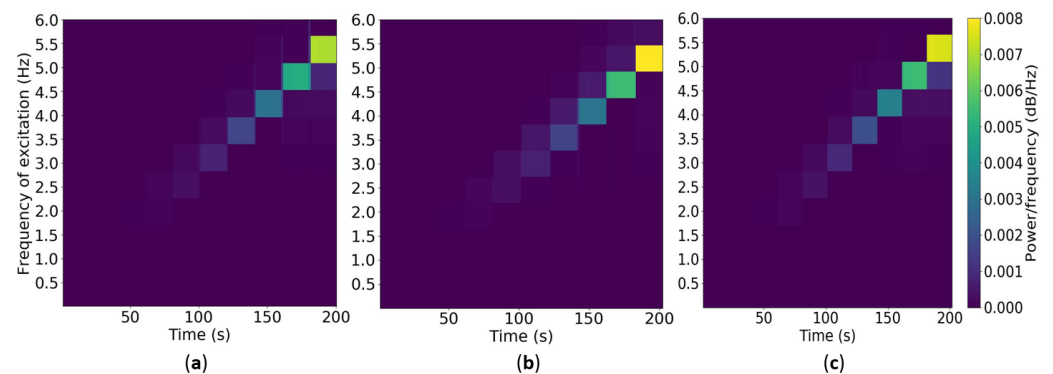


Figure 15. Spectrograms for the 0.10 cm displacement frequency chirp: (a) PCB L74 spectrogram. (b) ADXL355 RBP1 spectrogram. (c) ADXL355 RBP4 spectrogram.

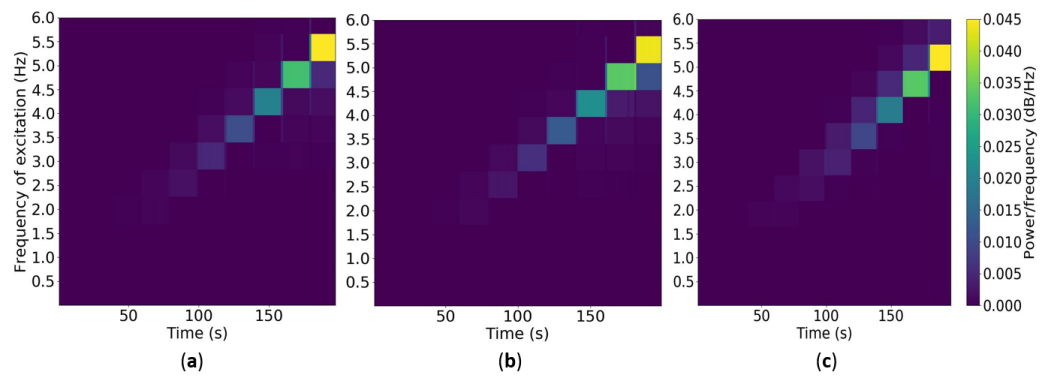


Figure 16. Spectrograms for the 0.25 cm displacement frequency chirp: (a) PCB L74 spectrogram. (b) ADXL355 RBP1 spectrogram. (c) ADXL355 RBP4 spectrogram.

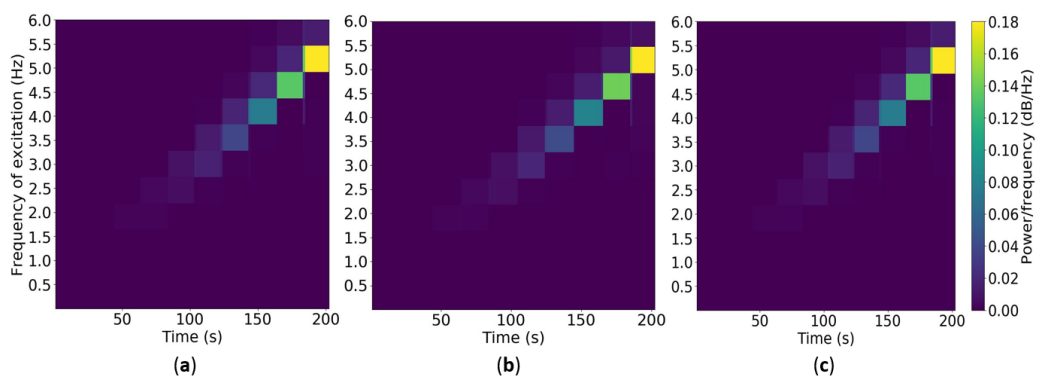


Figure 17. Spectrograms for the 0.50 cm displacement frequency chirp: (a) PCB L74 spectrogram. (b) ADXL355 RBP1 spectrogram. (c) ADXL355 RBP4 spectrogram.

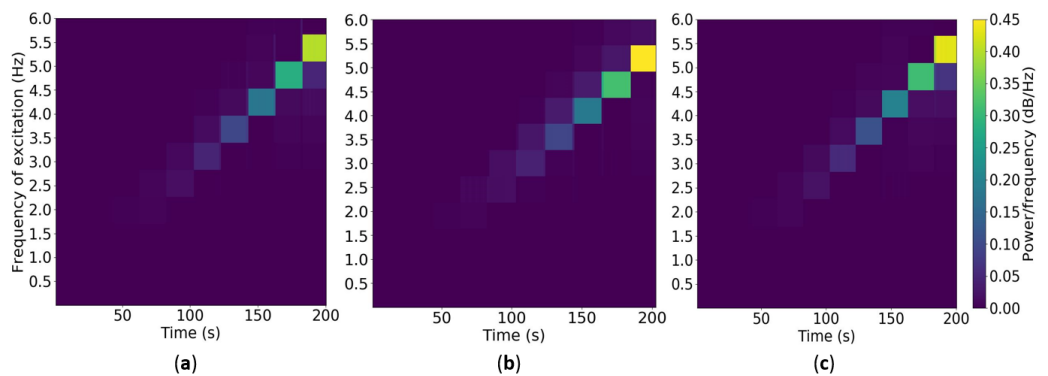


Figure 18. Spectrograms for the 0.75 cm displacement frequency chirp: (a) PCB L74 spectrogram. (b) ADXL355 RBP1 spectrogram. (c) ADXL355 RBP4 spectrogram.

4.1.2. Flexible Structure Monitoring

The modal identification of the dominant natural frequencies and mode shapes of the two-story structure provided five ambient vibration records. All ambient vibration datasets were post-processed to determine the best fitting time windows that would enable confident modal identification and MAC evaluation according to the information gathered. Figure 19 presents the dynamic response of the flexible structure in the frequency domain by the SHM systems in comparison. The SVD spectrum outlines the dominant vibration modes; the natural frequencies are identified from the representative singular value peaks, and the singular vectors associated with these peaks represent the mode shapes for the S1 values' frequency line. Otherwise, the S2 values' frequency line may include noise or

information about vibration modes less representative behind the natural dynamic response in the bandwidth. Thus, the S2 values' frequency line is neglected in this approach [34].

Both monitoring systems identified the first and second singular value peaks at 1.95 and 7.81 Hz, respectively. The mode shape vector related to each frequency notably represents the dynamic system response. Therefore, the 1.95 Hz natural frequency was adopted as the first dominant vibration mode, and the 7.81 Hz natural frequency was assumed as the second dominant vibration mode of the two-story structure. The modal identification results considering the measured dynamic response are shown in Table 7. Furthermore, the mode shapes detected from the SHM systems are depicted in Figure 20.

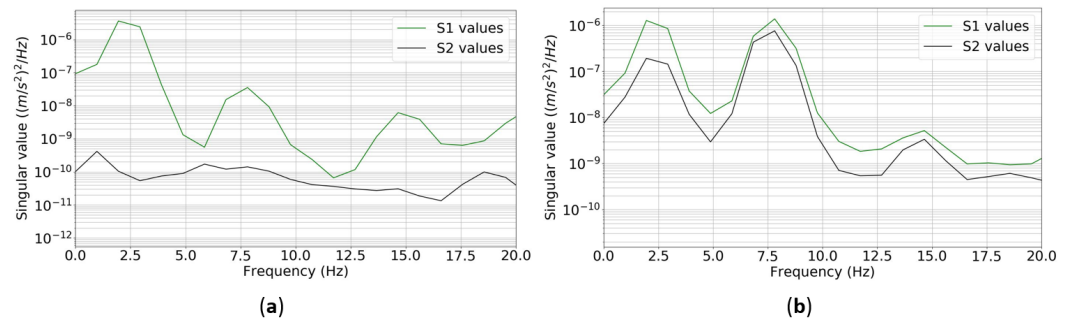


Figure 19. Dynamic response of the 2-DOF structure in the frequency domain: (a) SVD spectrum of the reference SHM system. (b) SVD spectrum of the low-cost SHM system.

Table 7. Natural frequencies and mode shapes identified of the flexible structure from both monitoring systems.

Vibration Mode 1				
Channel	Frequency (Hz)		Modal Coordinate	
	Reference System	Low-Cost System	Reference System	Low-Cost System
1	1.95	1.95	0.588	0.445
2			1.000	1.000
Vibration Mode 2				
Channel	Frequency (Hz)		Modal Coordinate	
	Reference System	Low-Cost System	Reference System	Low-Cost System
1	7.81	7.81	1.000	1.000
2			−0.759	−0.536

For the dynamic characterization results of the flexible structure, the modal identification performed through the low-cost SHM system demonstrates an accurate estimation. The natural frequencies reported from the low-cost SHM system were exactly equal considering the approach of the reference SHM system. For the mode shape validation of the WSN monitoring system, the MAC values were calculated to compare mode shapes estimated by the WSN and wired monitoring system. Figure 21 shows the MAC values calculated for the mode shapes' validation; the target vibration mode indicates the modal vectors determined by the reference SHM system, whereas the calculated vibration mode represents the modal vectors obtained from the low-cost SHM system. It was observed that the diagonal values of the MAC matrix were very close to the unity, demonstrating a high significant vibration mode correlation between mode shapes.

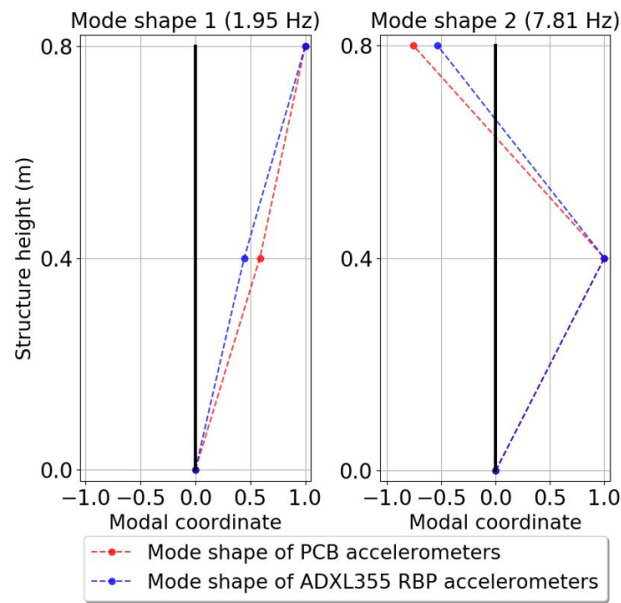


Figure 20. Mode shapes estimated by the monitoring systems.

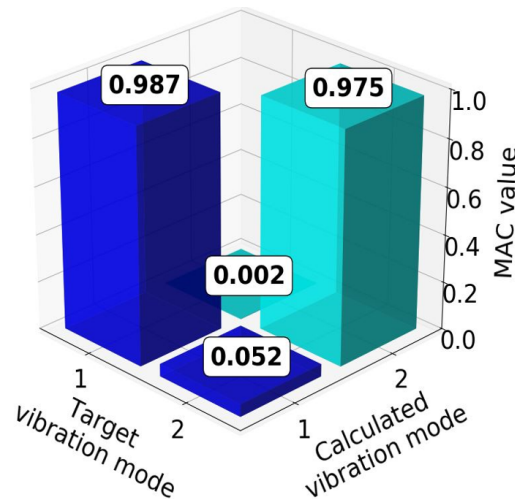


Figure 21. Modal assurance criterion for the mode shapes estimated.

The modal damping ratio related to the first dominant vibration mode was calculated by the logarithmic decrement method from the free-vibration dataset. For this purpose, a band-pass Butterworth filter, with cut-off frequencies at 0.10 Hz and 4.00 Hz, was implemented on free-vibration signals to hold the 1.95 Hz natural frequency content. Then, from a set of representative acceleration peaks, the logarithmic decrement was computed over every peak couple separated by six cycles to estimate the damping ratio. The same procedure was performed for the free-vibration signals on the DOF 1. Nevertheless, the damping ratio of the second dominant vibration mode was not considered due to its low modal contribution and the considerable disturbance produced by the filtering process [35]. Figure 22 indicates the exponential free-decay window selected from both SHM systems on the DOF 2 and a group of representative acceleration peaks from the ADXL355 RBP3 accelerometer.

By gathering a complete dataset of damping ratio results from measurement channels 1 and 2, the mean damping ratio and its coefficient of variation were calculated through both SHM systems and are indicated in Table 8. The mean damping ratio determined by the WSN monitoring system presented a relative error of 15.68% regarding the result from the wired monitoring system. The coefficients of variation of the mean damping ratio

from both monitoring systems did not exceed the state-of-the-art limit reported in [35], suggesting relative standard deviation or coefficient of variation values up to 53.0%.

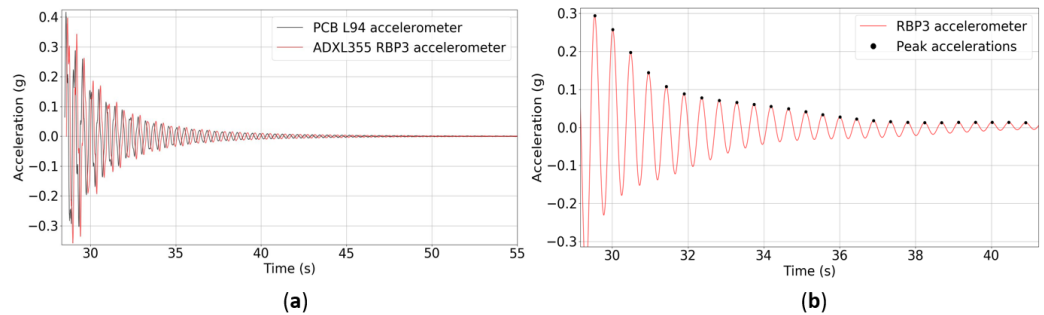


Figure 22. Free vibration response of the two-story structure for DOF 2: (a) Exponential free-decay window. (b) Representative acceleration peaks from the filtered free-vibration signal of the ADXL355 RBP3 accelerometer.

Table 8. Mean damping ratios and coefficients of variation calculated for both monitoring systems.

Vibration Mode 1			
Reference System		Low-Cost System	
Mean Damping Ratio (%)	Coefficient of Variation (%)	Mean Damping Ratio (%)	Coefficient of Variation (%)
2.022	46.8	2.339	36.8

4.2. Full-Scale Testing

The results obtained from the beam demolition monitoring and railway bridge monitoring are introduced below to assess the performance of the low-cost SHM system for large civil structures.

4.2.1. Beam Demolition Monitoring

The assessment of the dynamic response of the lightweight RC slab is presented for the span 1–2. The results reached for the rest of the spans from the prestressed concrete slab are extremely similar to the following analysis. Further information about the considerations and outcomes of other spans can be found in [36]. The ambient and forced vibration datasets during the hammer impact are shown in Figure 23. In these plots, the ambient vibration amplitude reached values up to 0.0022 g, and the peak detected for the forced vibration was 0.0040 g.

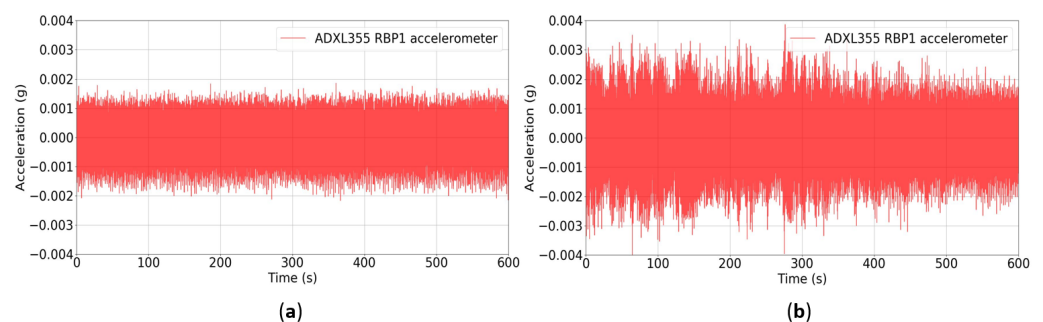


Figure 23. Vibration response from the span 1–2: (a) Ambient vibration record. (b) Forced vibration record during demolition work.

The dynamic response of the lightweight RC slab in the frequency domain, resulting from the ambient and forced vibration, was analyzed by the power spectral densities indicated in Figure 24. The relevant frequency content included a first frequency component between 9.84 and 11.5 Hz and a second frequency component located within a range of 21.9 and 22.7 Hz for both power spectral densities. In particular, as revealed by the power spectral density of forced vibration, the frequency impact of the Hilti demolition hammer on the check-in beam was detected by a sharp peak at 26.8 Hz.

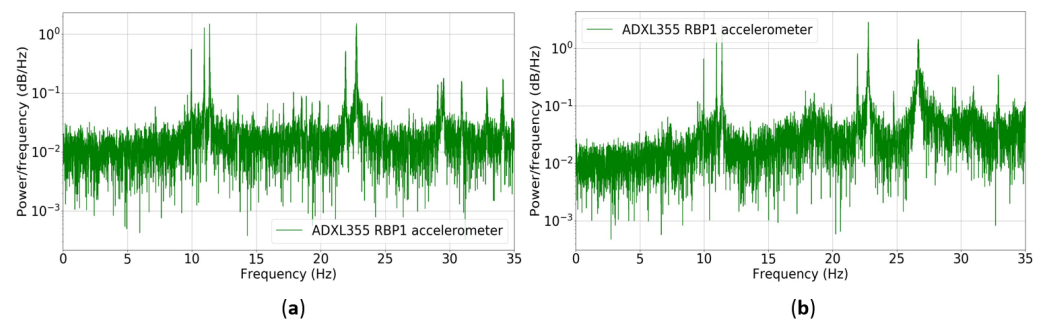


Figure 24. Dynamic response of the lightweight RC slab corresponding to the span 1–2: (a) Power spectral density of the ambient vibration. (b) Power spectral density of the forced vibration.

For the time–frequency distribution analysis, the energy content of the mentioned dominant frequencies is presented by the spectrograms in Figure 25. The natural frequency identification of the lightweight RC slab from the power spectral densities was verified by the first frequency lines detected in both spectrograms; moreover, the natural frequency ranges did not change significantly during the forced vibration record. Likewise, the impact frequency of the demolition hammer was observed notably at a frequency line very close to 27.0 Hz, as shown in the spectrogram of the forced vibration.

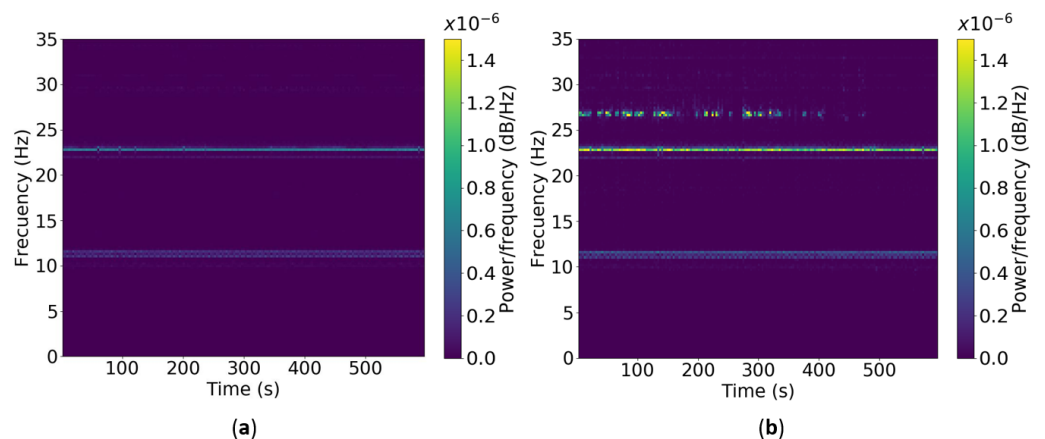


Figure 25. Time–frequency distribution of the response from the lightweight RC slab corresponding to the span 1–2: (a) Spectrogram of the ambient vibration. (b) Spectrogram of the forced vibration.

The first frequency component located between 9.84 and 11.5 Hz includes the fundamental natural frequency (10.0 Hz) of the same prestressed concrete slab reported in a previous official technical report, demonstrating an accurate estimation carried out from the low-cost SHM system. The demolition hammer was operating in a frequency bandwidth considerably separated from the dynamic response of the prestressed concrete slab. Therefore, the fundamental vibration mode did not experience resonance effects. It was observed that predominant vibration modes remained undamaged after demolition work. Thus, the stiffness and support conditions of the lightweight RC slab were preserved.

The wireless Internet connection and remote communication of the low-cost SHM system functioned permanently during the fieldwork under the ambient conditions and experimental setup design.

4.2.2. Railway Bridge Monitoring

The modal identification of the dominant natural frequencies and mode shapes of the railway bridge in vertical and transverse directions considered seventeen ambient vibration records. Analyzing the information collected, as mentioned in the flexible structure monitoring, every ambient vibration dataset was examined to select the best time windows for accurate modal identification and MAC evaluation. Due to the length of wired sensors and exposure to environmental conditions, the amplitude of the acceleration signal from the PCB L74 accelerometer was disturbed by noise. Thus, it was subjected to a high-pass Butterworth filter to remove the noise component from the data transmission system. Figure 26 presents a time window of the ambient transverse vibration signal from the structural response corresponding to the measurement channel 3. The ambient vibration amplitude for both PCB L74 and ADXL355 RBP2 accelerometers reached approximate values up to 0.0015 g.

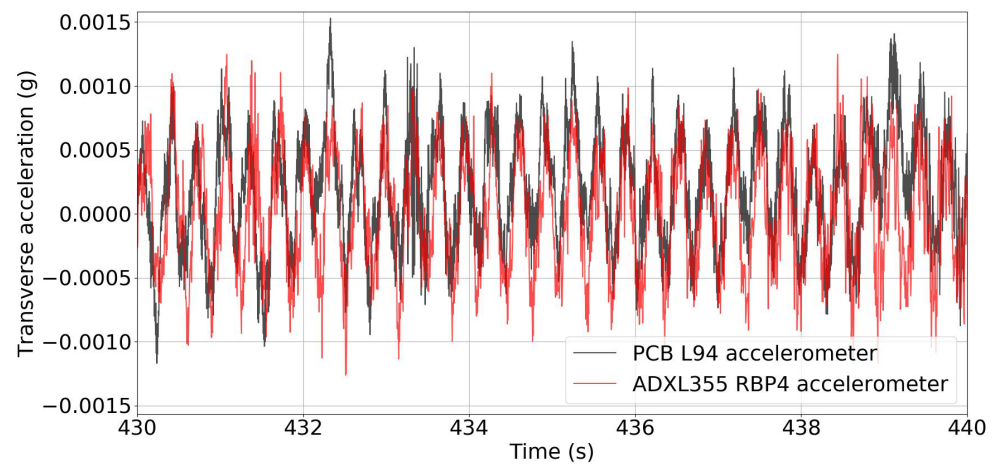


Figure 26. Transverse ambient vibration record of the railway bridge on measurement channel 3.

The vertical and transverse dynamic responses of the steel structure in the frequency domain from both SHM systems are shown in Figure 27 and Figure 28, respectively. For detecting the natural frequencies and mode shapes for each direction of analysis separately, the structural response was defined by the S1 values' frequency line of the SVD spectrum. In the vertical dynamic response of the railway bridge, the first singular value peak identified by both monitoring systems reached a frequency of 0.98 Hz. However, the mode shape vector associated with this frequency did not represent the dynamic response of the structure well. Next, for this first singular value peak, two singular value peaks were detected at 6.83 and 15.62 Hz frequencies for both monitoring systems. The mode shape vector related to each frequency remarkably represented the dynamic system response. Therefore, the 6.83 Hz natural frequency was suggested as the first dominant vibration mode, and the 15.62 Hz natural frequency was assumed as the second dominant vibration mode. In the transverse dynamic response of the railway bridge, the first and third singular value peaks identified by both monitoring systems indicated frequencies of 2.93 and 13.67 Hz, respectively. The mode shape vector related to each frequency significantly represented the dynamic system response. Therefore, the 2.93 Hz natural frequency was adopted as the first dominant vibration mode, and the 13.67 Hz natural frequency was suggested as the second dominant vibration mode. The second singular value peak detected was a frequency of 7.81 Hz, but its mode shape vector did not depict the dynamic response of the structure importantly. Finally, the fourth singular value peak distinguished by the reference

SHM system indicated a frequency of 17.58 Hz, and the low-cost SHM system pinpointed a frequency of 16.60 Hz. The magnitude discrepancy among both monitoring systems and the similarity of their mode shapes vectors regarding the first transverse vibration mode motivated us to dismiss this last frequency as an additional dominant vibration mode.

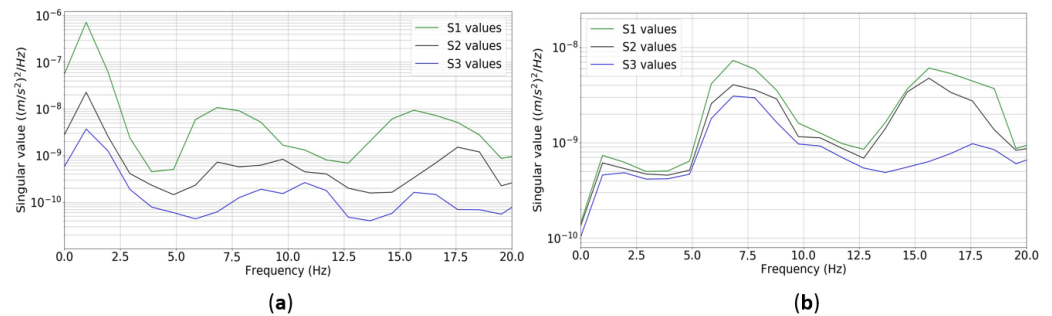


Figure 27. Vertical dynamic response of the 3-DOF structure in the frequency domain: (a) SVD spectrum of the reference SHM system. (b) SVD spectrum of the low-cost SHM system.

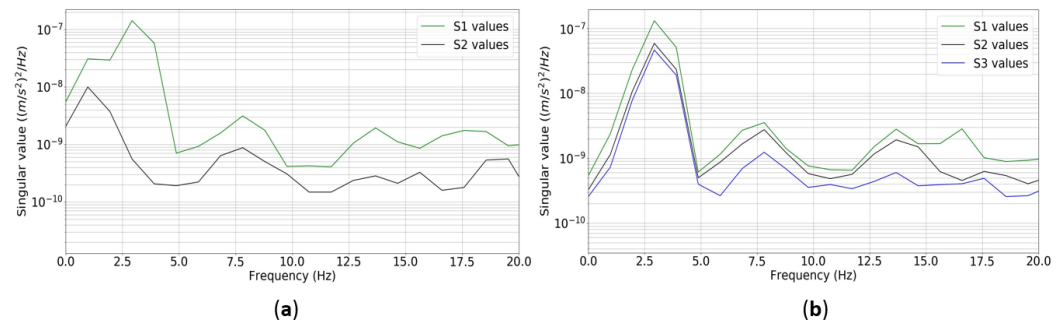


Figure 28. Transverse dynamic response of the 3-DOF structure in the frequency domain: (a) SVD spectrum of the reference SHM system. (b) SVD spectrum of the low-cost SHM system.

The vertical and transverse modal identification results considering the measured dynamic responses are shown in Table 9 and Table 10, respectively. Moreover, the mode shapes related to both directions of analysis from the SHM systems are depicted in Figures 29 and 30.

Table 9. Vertical natural frequencies and mode shapes identified of the steel structure by both monitoring systems.

Vertical Vibration Mode 1				
Channel	Frequency (Hz)		Modal Coordinate	
	Reference System	Low-cost System	Reference System	Low-cost System
1			0.751	0.379
2	6.83	6.83	1.000	1.000
3			0.660	0.084
Vertical Vibration Mode 2				
Channel	Frequency (Hz)		Modal Coordinate	
	Reference System	Low-Cost System	Reference System	Low-Cost System
1			−0.963	−0.476
2	15.62	15.62	0.301	−0.022
3			1.000	1.000

Table 10. Transverse natural frequencies and mode shapes identified of the steel structure by both monitoring systems.

Transverse Vibration Mode 1				
Channel	Frequency (Hz)		Modal Coordinate	
	Reference System	Low-Cost System	Reference System	Low-Cost system
1	2.93	2.93	0.644	0.602
2			1.000	0.882
3			0.644	1.000

Transverse Vibration Mode 2				
Channel	Frequency (Hz)		Modal Coordinate	
	Reference System	Low-Cost System	Reference System	Low-Cost System
1	13.67	13.67	−1.000	−0.844
2			0.216	0.201
3			1.000	1.000

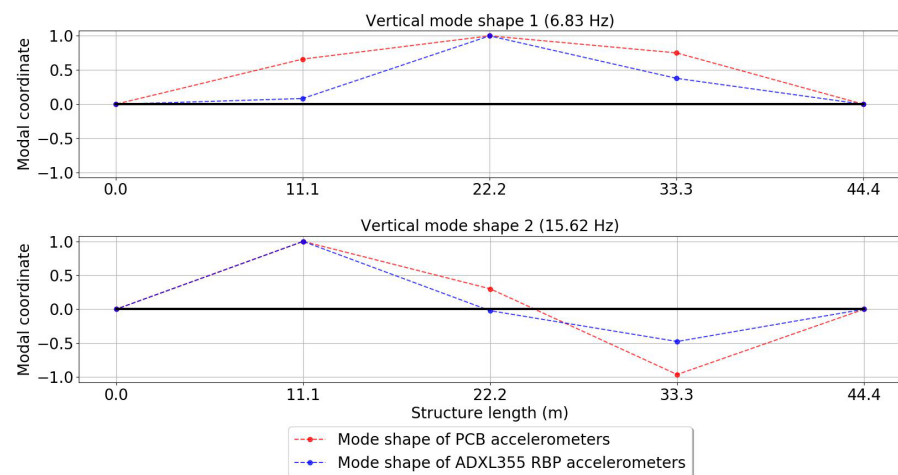


Figure 29. Vertical mode shapes of the railway bridge estimated by the monitoring systems.

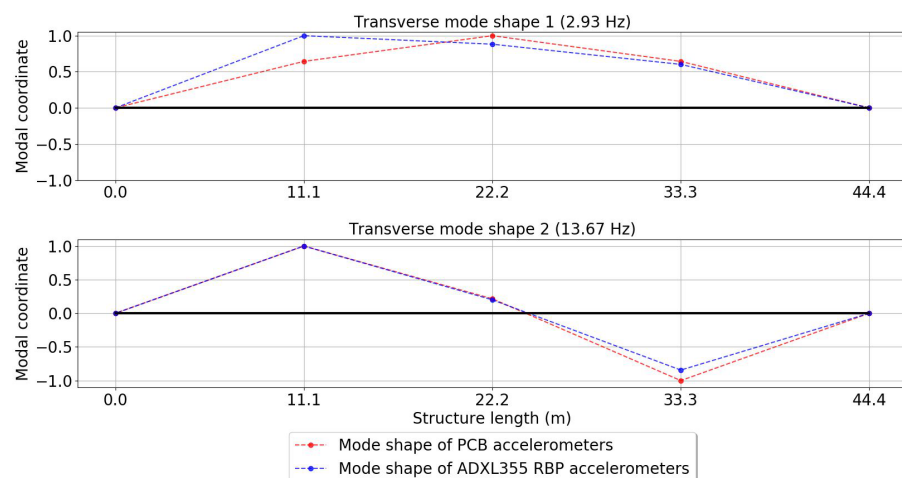


Figure 30. Transverse mode shapes of the railway bridge estimated by the monitoring systems.

The modal identification carried out by the low-cost SHM system had a good estimation. As occurred in the flexible structure monitoring, the natural frequencies reported from

the low-cost SHM system were exactly equal considering the approach of the reference SHM system. For the mode shapes' validation from the WSN monitoring system, the MAC values were calculated for the vertical and transverse vibration mode correlation (Figure 31). The diagonal values of the vertical modes MAC matrix were relatively close to unity. The consistency of the vertical vibration mode 1 was really close to the MAC acceptance level, and the correlation of the vertical vibration mode 2 demonstrated a reliable outcome concerning the state-of-the-art acceptance criterion considered in the present study. On the other hand, the diagonal values from the transverse modes MAC matrix were close to unity. The consistency of the transverse vibration modes 1 and 2 was high.

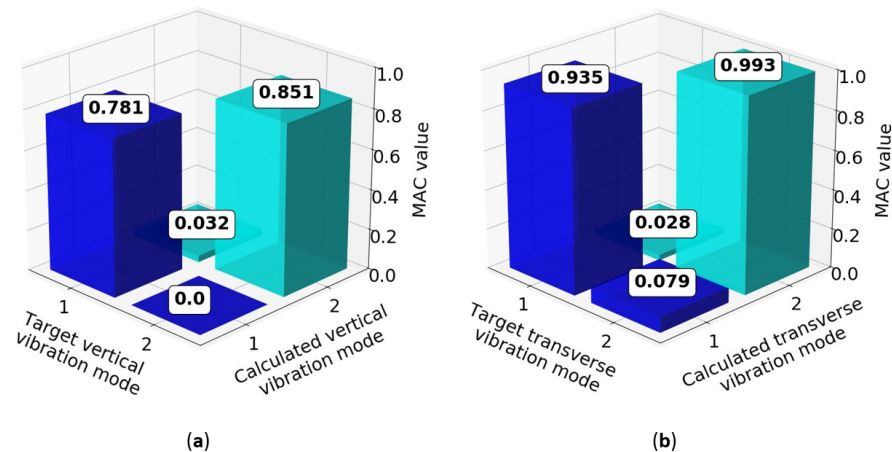


Figure 31. Modal assurance criteria for the mode shapes estimated of the structure: (a) Vertical mode correlation. (b) Transverse mode correlation.

The limited vibration mode correlation with the vertical mode shapes of the structure arose because of the vibration dataset asynchrony detected in the low-cost SHM system performance.

As an example of the different kinds of trains tested, the transverse vibration record of a 48 km/h empty-load train from measurement channel 3 is presented in Figure 32. For transverse forced vibrations of this train tested, the absolute maximum acceleration detected by the PCB L94 accelerometer was 1.662 g, and the absolute maximum acceleration measured from the ADXL355 RBP4 accelerometer was 1.464 g.

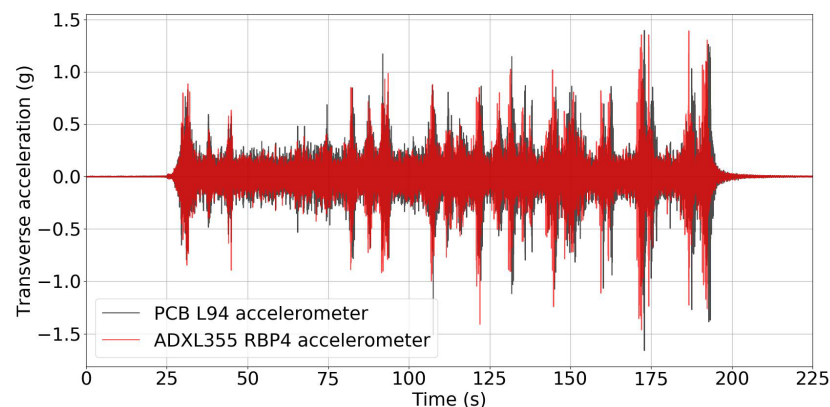


Figure 32. Transverse forced vibration record of a 48 km/h empty-load train on measurement channel 3.

The modal damping ratio, related to the first vertical and transverse dominant vibration modes, was calculated using the logarithmic decrement method to analyze sixteen forced and free-vibration datasets. The vertical and transverse free-vibration responses of

the railway bridge of a 48 km/h empty-load train and a 52 km/h empty-load train, respectively, were selected to calculate the damping ratios since the free-decay signals thereof were well-defined exponentially. As explained for the damping estimation of the flexible structure, the Butterworth signal processing filter was used on the free-vibration signals using the band-pass specification based on the frequencies of interest. In the damping estimation for the 6.83 Hz vertical vibration mode, the cut-off frequencies were 5.0 and 8.0 Hz. While for the 2.93 Hz transverse vibration mode, the cut-off frequencies were 1.0 and 5.0 Hz. Figure 33 indicates the transverse exponential free-decay window extracted from both SHM systems on the DOF 4 of the steel bridge and a group of representative acceleration peaks from the ADXL355 RBP4 accelerometer. Once the vertical and transverse free-vibration signals from all the measurements channels got filtered, the damping ratio of the first vertical and transverse vibration modes was estimated by the logarithmic decrement method following the procedure stated earlier in the small-scale testing damping estimation.

After elaborating a comprehensive dataset from the damping ratios estimated, the mean damping ratio and its coefficient of variation, related to the vertical and transverse vibration modes, were calculated with both SHM systems and are indicated in Table 11. The vertical mean damping ratio determined from the low-cost SHM system had a relative error of 2.68% compared to the result of the reference SHM system. On the other hand, the transverse mean damping ratio calculated by the low-cost SHM system presented a relative error of 2.51% regarding the approach from the reference SHM system. The vertical and transverse mean damping ratio variation from both SHM monitoring systems was within the state-of-the-art limit considered previously.

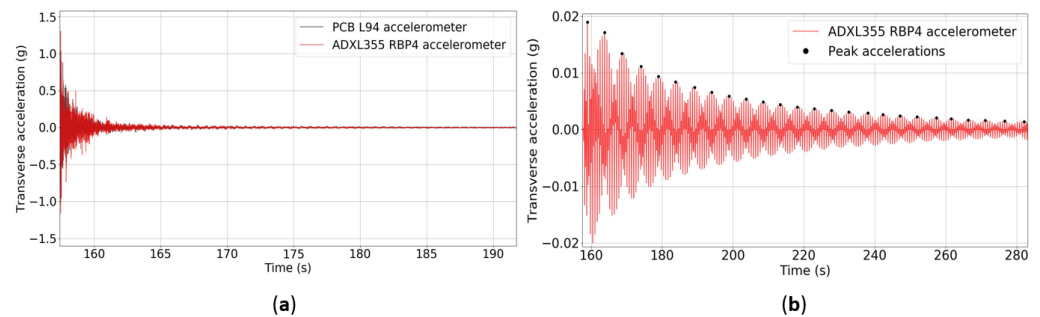


Figure 33. Transverse free-vibration response of the steel structure for DOF 4: (a) Exponential free-decay window. (b) Representative acceleration peaks from the filtered free-vibration signal of the ADXL355 RBP4 accelerometer.

Table 11. Mean damping ratios and coefficients of variation calculated for both monitoring systems.

Vertical Vibration Mode 1			
Reference System		Low-Cost System	
Mean Damping Ratio (%)	Coefficient of Variation (%)	Mean Damping ratio (%)	Coefficient of Variation (%)
3.54	19.2	3.63	22.8
Transverse Vibration Mode 1			
Reference System		Low-cost System	
Mean Damping Ratio (%)	Coefficient of Variation (%)	Mean Damping ratio (%)	Coefficient of Variation (%)
1.553	21.1	1.514	24.4

Distances larger than approximately 20 m between a measuring node and the base station interrupted the permanent wireless Internet connection and continuous remote communication. To effectively establish the wireless connection and remote access on measurement channels 1 and 2, the Wi-Fi router was relocated to the closest position to both spots to verify the functioning of the measuring nodes by a smartphone login.

5. Conclusions

A low-cost Structural Health Monitoring (SHM) system was designed and implemented in small- and full-scale tests. The Wireless Sensor Network (WSN), the base station, and the standard dynamical identification techniques enabled monitoring the structural responses to ambient, forced, and free-vibrations; and accomplished the dynamic characterization of civil structures in pseudo-real time. The vibration data and modal parameters estimated from the low-cost SHM system were compared to a reference SHM system to validate the performance of the WSN monitoring strategy with a deterministic approach.

For the small-scale testing, the data vibration analysis and comparison in the frequency chirps from the shaking table tests were conducted based on ten different frequency levels (from 0.5 to 5.0 Hz) and four displacement levels (from 0.10 to 0.75 cm). It was observed that RMS errors decreased for the evaluation carried out on the resampled acceleration signals. The WSN monitoring system detected maximum accelerations associated with RMS error of up to 0.032 g, and the mean of the highest 100 resampled acceleration peaks displayed RMS error of up to 0.017 g. The dynamic characterization of the tested flexible structure showed that the low-cost SHM system effectively measured ambient vibrations greater or equal to 0.0008 g and identified precisely the first dominant natural frequencies within the frequency range between 0 and 10.0 Hz. Regarding the mode shape's correlation with the traditional SHM system, the modal assurance criterion (MAC) values were higher than 0.970. The estimated mean damping ratio was 2.339%, and its coefficient of variation was 36.8%.

In the full-scale testing, the relevant natural frequencies of the lightweight RC slab were reliably estimated and monitored during the demolition work through the frequency analysis involving the power spectral densities and time–frequency distributions. The demolition and replacement of the original RC check-in beam did not result in structural disturbance to the prestressed concrete slab. From the dynamic characterization of the railway bridge, the low-cost SHM system appropriately measured ambient vibrations higher or equivalent to 0.0015 g, thereby permitting excellent identification of the first dominant vertical and transverse natural frequencies within the frequency range among 0 and 20.0 Hz. For the mode shape's correlation with the traditional SHM system, the MAC values ranged between 0.781 and 0.993. The estimated mean damping ratios were 1.514% and 3.630%, with coefficients of variation of 24.4% and 22.8%, respectively. The mean damping ratios of the small- and full-scale experimental tests represented low damping values, so the flexible structure and the railway bridge were recognized as lightly damped structures. Thus, besides the well-separated vibration modes obtained and white noise assumption for ambient vibrations, the frequency domain decomposition (FDD) technique was considered an accurate approach for the dynamic characterization performed in this study. To achieve higher accuracy with the modal identification technique employed, improving the vibration dataset synchronization of the WSN monitoring system would be ideal considering the notable performance of the low-cost accelerometers.

The small investment required for the low-cost SHM system and its features support its implementation over existing WSN monitoring systems. This alternative WSN system supports a higher accelerometer resolution (20-bit) than the three previously mentioned WSN monitoring systems. The ADXL355 accelerometer covers a wide measurement range of ± 2.0 g for dynamic characterization from vibration data, as two of the monitoring proposals used in comparison do. However, the measuring node of the low-cost SHM system requires the highest cabled power supply (8.3 V) among these monitoring systems. Regarding the costs, the alternative WSN system has the lowest estimated cost per node

of USD 73.5 compared to the rest of the wireless SHM systems. Hence, the properties of the low-cost SHM system may provide a competent, cheap methodology for the SHM of civil structures.

The on-field arrangement of the low-cost SHM system demonstrated a relevant capability for monitoring the structural response through a permanent wireless Internet connection and remote communication to distances of up to 20 m between the measuring node and base station. This research combined the implementation of low-cost, easy-to-use electronic devices; the practicality of laboratory and on-field experimental setups; and the computing of standard dynamical identification techniques in order to efficiently characterize the structural dynamic properties of civil infrastructure using an extensive, flexible SHM system. Future research directions may extend the presented standard dynamical identification technique by adding vibration-based damage detection methods, finite element model updating, and digital twins algorithms that examine the structural health in ambient conditions or in response to natural hazards in real-time.

Author Contributions: Conceptualization, D.C.-R., A.R.O. and A.G.; methodology, D.C.-R., A.R.O. and A.G.; formal analysis, D.C.-R. and A.R.O.; software, D.C.-R. and C.C.; writing—original draft preparation, D.C.-R., A.R.O. and A.G.; writing—review and editing, D.C.-R. and A.R.O. All authors have read and agreed to the published version of the manuscript.

Funding: This research received no external funding.

Institutional Review Board Statement: Not applicable.

Informed Consent Statement: Not applicable.

Data Availability Statement: The data presented in this study might be available on reasonable request from the corresponding author.

Acknowledgments: The authors would like to thank Universidad del Norte for providing the National Instrument data acquisition system and PCB Piezotronics accelerometers for the instrumentation of large-scale civil structures.

Conflicts of Interest: The authors declare no conflict of interest.

References

1. Farrar, C.R.; Worden, K. An introduction to structural health monitoring. *Philos. Trans. R. Soc. A Math. Phys. Eng. Sci.* **2007**, *365*, 303–315. [[CrossRef](#)] [[PubMed](#)]
2. Yuen, K.V.; Au, S.K.; Beck, J.L. Two-stage structural health monitoring approach for phase I benchmark studies. *J. Eng. Mech.* **2004**, *130*, 16–33. [[CrossRef](#)]
3. Chen, H.P.; Ni, Y.Q. *Structural Health Monitoring of Large Civil Engineering Structures*; Wiley Online Library: Hoboken, NJ, USA, 2018.
4. Nunez, T.; Boroschek, R.; Larrain, A. Validation of a construction process using a structural health monitoring network. *J. Perform. Constr. Facil.* **2013**, *27*, 270–282. [[CrossRef](#)]
5. Rice, J.A.; Spencer, B.F., Jr. *Flexible Smart Sensor Framework for Autonomous Full-Scale Structural Health Monitoring*; Technical Report; Newmark Structural Engineering Laboratory, University of Illinois at Urbana-Champaign: Urbana, IL, USA, 2009.
6. Cho, S.; Yun, C.B.; Lynch, J.P.; Zimmerman, A.T.; Spencer, B.F., Jr.; Nagayama, T. Smart wireless sensor technology for structural health monitoring of civil structures. *Steel Struct.* **2008**, *8*, 267–275.
7. Cao, J.; Liu, X. *Wireless Sensor Networks for Structural Health Monitoring*; Springer: Berlin/Heidelberg, Germany, 2016.
8. Moreu, F.; Li, X.; Li, S.; Zhang, D. Technical specifications of structural health monitoring for highway bridges: New Chinese structural health monitoring code. *Front. Built Environ.* **2018**, *4*, 10. [[CrossRef](#)]
9. Lynch, J.P.; Loh, K.J. A summary review of wireless sensors and sensor networks for structural health monitoring. *Shock Vib. Dig.* **2006**, *38*, 91–130. [[CrossRef](#)]
10. Sohn, H.; Farrar, C.R.; Hemez, F.M.; Shunk, D.D.; Stinemates, D.W.; Nadler, B.R.; Czarnecki, J.J. *A Review of Structural Health Monitoring Literature: 1996–2001*; Los Alamos National Laboratory: Los Alamos, NM, USA, 2003; Volume 1.
11. Javadinasab Hormozabad, S.; Gutierrez Soto, M.; Adeli, H. Integrating structural control, health monitoring, and energy harvesting for smart cities. *Expert Syst.* **2021**, *38*, e12845. [[CrossRef](#)]
12. Melendez, A.; Caballero-Russi, D.; Gutierrez Soto, M.; Giraldo, L.F. Computational models of community resilience. *Nat. Hazards* **2021**, 1–32. [[CrossRef](#)]

13. Hartnagel, B.A.; O'Connor, J.; Yen, W.H.; Clogston, P.; Çelebi, M. Planning and implementation of a seismic monitoring system for the Bill Emerson Memorial Bridge in Cape Girardeau, MO. In Proceedings of the Structures Congress 2006: Structural Engineering and Public Safety, St. Louis, MO, USA, 18–21 May 2006; pp. 1–8.
14. Ni, Y.; Xia, H.; Ko, J. Structural performance evaluation of Tsing Ma Bridge deck using long-term monitoring data. *Mod. Phys. Lett. B* **2008**, *22*, 875–880. [[CrossRef](#)]
15. Jang, S.; Jo, H.; Cho, S.; Mechtov, K.; Rice, J.A.; Sim, S.H.; Jung, H.J.; Yun, C.B.; Spencer, B.F., Jr.; Agha, G. Structural health monitoring of a cable-stayed bridge using smart sensor technology: Deployment and evaluation. *Smart Struct. Syst.* **2010**, *6*, 439–459. [[CrossRef](#)]
16. Zonta, D.; Wu, H.; Pozzi, M.; Zanon, P.; Ceriotti, M.; Mottola, L.; Picco, G.P.; Murphy, A.L.; Guna, S.; Corra, M. Wireless sensor networks for permanent health monitoring of historic buildings. *Smart Struct. Syst.* **2010**, *6*, 595–618. [[CrossRef](#)]
17. Kim, S.; Pakzad, S.; Culler, D.; Demmel, J.; Fenves, G.; Glaser, S.; Turon, M. Health monitoring of civil infrastructures using wireless sensor networks. In Proceedings of the 6th International Conference on Information Processing in Sensor Networks, Cambridge, MA, USA, 25–27 April 2007; pp. 254–263.
18. Chopra, A.K. *Dynamics of Structures*; Pearson Education: London, UK, 2012.
19. Brincker, R.; Ventura, C.E.; Andersen, P. Damping estimation by frequency domain decomposition. In Proceedings of the IMAC 19: A Conference on Structural Dynamics, Kissimmee, FL, USA, 5–8 February 2001; Society for Experimental Mechanics: Bethel, CT, USA, 2001; pp. 698–703.
20. Pioldi, F.; Ferrari, R.; Rizzi, E. A refined FDD algorithm for Operational Modal Analysis of buildings under earthquake loading. In Proceedings of the 26th International Conference on Noise and Vibration Engineering, Leuven, Belgium, 15–17 September 2014; Volume 1, pp. 3353–3368.
21. Brincker, R.; Zhang, L.; Andersen, P. Modal identification from ambient responses using frequency domain decomposition. In Proceedings of the 18th International Modal Analysis Conference (IMAC), San Antonio, TX, USA, 7–10 February 2000.
22. Pastor, M.; Binda, M.; Harčarik, T. Modal assurance criterion. *Procedia Eng.* **2012**, *48*, 543–548. [[CrossRef](#)]
23. Rainieri, C.; Fabbrocino, G. *Operational Modal Analysis of Civil Engineering Structures*; Springer: Berlin/Heidelberg, Germany, 2014.
24. Tischer, H.; Thomson, P.; Marulanda, J. Comparación de tres transformadas para distribuciones tiempo-frecuencia por medio de su aplicación a registros de vibraciones ambientales. *Ingeniería Compet.* **2007**, *9*, 21–32. [[CrossRef](#)]
25. Raspberry Pi Foundation. *Raspberry Pi 3 Model B+*; Technical Report; Raspberry Pi Foundation: Cambridge, UK, 2018.
26. Allied Electronics & Automation. Raspberry Pi RASPBERRY PI 3 MODEL B+. 2020. Available online: <https://en-co.alliedelec.com/product/raspberry-pi/raspberry-pi-3-model-b-/71131895/?src=raspberrypi> (accessed on 5 August 2020).
27. Analog Devices. *Data Sheet ADXL354/ADXL355*; Technical Report; Analog Devices Inc.: Norwood, MA, USA, 2018.
28. Analog Devices. EVAL-ADXL35X. 2020. Available online: <https://www.analog.com/en/design-center/evaluation-hardware-and-software/evaluation-boards-kits/EVAL-ADXL35X.html#eb-overview> (accessed on 14 May 2020).
29. ElectronicWings. RASPBERRY PI I2C. 2019. Available online: <https://www.electronicwings.com/raspberry-pi/raspberry-pi-i2c> (accessed on 19 December 2019).
30. Mills, D.L. Internet time synchronization: The network time protocol. *IEEE Trans. Commun.* **1991**, *39*, 1482–1493. [[CrossRef](#)]
31. National Instruments. *NI 9234 Datasheet*; Technical Report; National Instruments Inc.: Austin, TX, USA, 2015.
32. Quanser. *Shake Table II Datasheet*; Technical Report; Quanser Inc.: Markham, ON, Canada, 2019.
33. Hilti. *Manual Martillo Rompedor TE 1000-AVR/TE 1500-AVR*; Technical Report; Hilti Corporation: Schaan, Liechtenstein, 2013.
34. Freire Obregón, C. Implementación y Validación del método Mejoramiento de Descomposición en el Dominio de la Frecuencia (EFDD) para la Identificación de los Parámetros Modales de Estructuras genéricas Utilizando Ruido Ambiente. Estudio del Rango de Aplicabilidad en función del Modelo Estructural y las Condiciones de uso. Master's Thesis, Universidad de Las Palmas de Gran Canaria, Las Palmas, Spain, 2011.
35. Magalhães, F.; Cunha, Á.; Caetano, E.; Brincker, R. Damping estimation using free decays and ambient vibration tests. *Mech. Syst. Signal Process.* **2010**, *24*, 1274–1290. [[CrossRef](#)]
36. Caballero, D. Caracterización Dinámica de Estructuras Empleando un Sistema de Monitoreo de Salud Estructural de bajo Costo. Master's Thesis, Universidad del Norte, Barranquilla, Colombia, 2021.